Space-time dynamics of depositional systems: Experimental evidence and theoretical modeling of heavy-tailed statistics

Vamsi Ganti,[1,2] Kyle M. Straub,[3] Efi Foufoula-Georgiou,[1,2] and Chris Paola[1,4]

Received 3 October 2010; revised 10 February 2011; accepted 17 February 2011; published 12 May 2011.

[1] In depositional systems, channels migrate from one location to another, causing erosion and deposition at any given point in the domain. The durations of depositional and erosional events, as well as their magnitudes, control the structure of the stratigraphic record. In this study, we use high-resolution temporal surface elevation data from a controlled experiment to quantify the probability distributions of the processes that govern the evolution of depositional deltaic systems. Heavy-tailed statistics of erosional and depositional events are documented, indicating that a small but significant chance exists for the occurrence of extreme events. We show that the periods of inactivity, when neither deposition nor erosion occurs, follow a truncated Pareto distribution whose truncation scale is set by the mean characteristic avulsion time scale in the system. Further, we show that the heavy tails in the magnitudes of the erosional and depositional events are not preserved in the stratigraphic record, resulting instead in an exponential distribution for the bed sediment thickness. It is also shown that the temporal evolution of surface elevation exhibits self-similarity with a nonlinear spectrum of scaling exponents (multifractality) quantifying the complex dynamics of the system. Finally, we show how the results of this study can lead to improved diffusional models for surface evolution using the tools of fractional calculus.

Citation: Ganti, V., K. M. Straub, E. Foufoula-Georgiou, and C. Paola (2011), Space-time dynamics of depositional systems: Experimental evidence and theoretical modeling of heavy-tailed statistics, *J. Geophys. Res.*, *116*, F02011, doi:10.1029/2010JF001893.

1. Introduction

[2] The architecture of stratigraphy is a function of three characteristics of depositional systems: (1) the topography of an actively deforming surface, (2) the dynamics of the deforming surface, and (3) the rate of net deposition [*Paola et al.*, 2009; *Sheets et al.*, 2002, 2007; *Strong and Paola*, 2008]. As all three of these properties are influenced by environmental conditions (e.g., climate and tectonics) the architecture of stratigraphy in sedimentary basins contains a vast amount of data that could be used to quantitatively reconstruct paleolandscape dynamics across many time scales [*Ager*, 1973; *Paola*, 2000; *Allen*, 2008]. Quantitative analysis of stratigraphy exposed in outcrops or imaged in seismic data coupled to numerical modeling of sedimentary basin filling has blossomed over the last 30 years, initiating with the pioneering works by *Leeder* [1978] and *Allen* [1978]. The general goal for many of these studies was to develop tools to invert stratigraphic data for paleoenvironmental conditions. This exercise has proved to be a difficult venture. Of the many challenges associated with inverting the stratigraphic record one of the greatest is characterizing how large-magnitude but infrequent events (e.g., avulsions, storms, floods) influence the dynamics of depositional systems and how this information gets stored in stratigraphy. Characterizing these large magnitude infrequent events is challenging because many of these events have recurrence intervals with intermediate time scales (10^1–10^4 years) which make them difficult to study directly or to constrain using dating techniques [*Sheets et al.*, 2002]. In this paper we used data from a physical experiment on a fluvial system in an experimental basin experiencing relative subsidence to characterize statistics associated with the fluvial dynamics that are dominant in these intermediate time scales (referred to as "mesoscale" dynamics by *Sheets et al.* [2002]) of depositional systems.

[3] As discussed by *Paola* [2000] and *Sheets et al.* [2002] the time scales associated with mesoscale dynamics lie between two deterministic end-members. *Sheets et al.* [2002] provide a heuristic definition for the mesoscale time range as one which has a lower bound given by the "short" time scale (time scales of evolution of bedforms and bars) on which channels behave coherently and deterministically in

[1]St. Anthony Falls Laboratory and National Center for Earth-surface Dynamics, University of Minnesota, Minneapolis, Minnesota, USA.
[2]Department of Civil Engineering, University of Minnesota, Minneapolis, Minnesota, USA.
[3]Department of Earth and Environmental Sciences, Tulane University, New Orleans, Louisiana, USA.
[4]Department of Geology and Geophysics, University of Minnesota, Minneapolis, Minnesota, USA.

0148-0227/11/2010JF001893

response to the sediment routing system, and an upper bound given by the "long" time scale (time scales of basinwide deposition) on which autocyclic variability sums to produce the average behavior represented in stratigraphic models [*Paola*, 2000]. In many cases, the mesoscale time range is the domain of stochastic behavior associated with avulsion and reorganization of the fluvial system. This has been recognized at least since the work of *Leeder* [1978] who developed the first physically based quantitative model for alluvial architecture. In this model, fluvial basins were filled by channels avulsing at a constant frequency to random locations. Since the publication of this model many additional alluvial architecture models have been proposed which characterize various properties of the stochastic depositional dynamics (avulsion frequency, avulsion jump length, etc.) through random numbers generated from probability density functions of various shapes [*Alexander and Leeder*, 1987; *Mackey and Bridge*, 1995; *Pyrcz et al.*, 2005]. These models have in part been motivated by field observations of stratigraphy in which depositional elements are at least partially organized in a stochastic fashion [*Hajek et al.*, 2010; *Straub et al.*, 2009; *Pelletier and Turcotte*, 1997]. However, at present few time series of depositional dynamics exist to aid the identification of the type and shape of probability distributions which should be used for modeling the mesoscale dynamics that result in stochastic stratigraphy.

[4] The focus of this study is to characterize the probability distributions that describe the dynamics of depositional systems using a time series of elevation recorded at several spatial transects during a physical experiment on delta evolution in a net aggradation setting. During this experiment, elevation was monitored at a temporal frequency comparable to the time scale of the system's mesoscale dynamics and over a duration long enough to generate reliable statistics on the magnitude of elevation increments. In particular, this study addresses two issues: (1) which probability distributions describe the processes that govern the depositional dynamics of the system and (2) to what degree do physical mechanisms constrain the occurrence of extremes and how are these constraints reflected in the probability distributions of the processes? Answering these two questions will not only improve our ability to characterize the statistics of depositional systems but will also aid the community in filtering environmental signals preserved in stratigraphy.

[5] The paper is structured as follows. In section 2, we give a brief outline of the experimental data analyzed in this study. In section 3, the variables whose statistical characteristics are studied are defined along with their notation. In sections 4 and 5, a statistical analysis of the random variables which govern the surface dynamics and preserved stratigraphic record in the experimental delta are presented. Having established the non-Gaussian form of the probability distributions of the processes involved, in section 6 the self-similar structure of surface evolution is characterized using higher-order statistical structure function analysis. In section 7, we address the question of what physical mechanisms constrain the occurrence of extremes in depositional systems and how these constraints are reflected in the probability distributions of the random variables studied. Preliminary thoughts on continuum models for surface evolution of depositional systems consistent with the documented probability distributions for erosional, depositional and inactivity events are presented in section 8. Finally, conclusions are drawn in section 9.

2. Experimental Setting

[6] The experiment discussed in this paper (DB-03) was performed and originally documented by *Sheets et al.* [2007]. The main focus of the work of *Sheets et al.* [2007] was documenting the creation and preservation of channel-form sand bodies in alluvial systems. Since this initial publication, data from the DB-03 experiment have been utilized in studies on compensational stacking of sedimentary deposits [*Straub et al.*, 2009] and clustering of sand bodies in fluvial stratigraphy [*Hajek et al.*, 2010]. In this section we provide a short description of the experimental setup. For a more detailed description see *Sheets et al.* [2007].

[7] The motivation for the DB-03 experiment was to obtain detailed records of fluvial processes, topographic evolution and stratigraphy, with sufficient spatial and temporal resolution to observe and quantify the deposition of channel sand bodies. The experiment was performed in the Delta Basin at St. Anthony Falls Laboratory at the University of Minnesota. This basin is 5 m by 5 m and 0.61 m deep (Figure 1a). Accommodation is created in the Delta Basin by slowly increasing the base level by way of a siphon-based ocean controller. This system allows for the control of base level with millimeter resolution [*Sheets et al.*, 2007].

[8] The experiment included an initial build-out phase in which sediment and water were mixed in a funnel and fed into one corner of the basin while base level remained constant. The delta was allowed to prograde into the basin and produced an approximately radially symmetrical fluvial system. After the system prograded 2.5 m from source to shoreline a base level rise was initiated. Subsidence in the Delta Basin was simulated via a gradual rise in base level, at a rate equal to the total sediment discharge (Q_s) divided by the desired fluvial system area. This sediment feed rate allowed the shoreline to be maintained at an approximately constant location through the course of the experiment. A photograph of the experimental deposit, including the topographic measurement lines, is shown in Figure 1. *Sheets et al.* [2007] used a sediment mixture of 70% 120 μm silica sand and 30% bimodal (190 μm and 460 μm) anthracite coal.

[9] Topography was measured with a subaerial laser topography scanning system, similar to the system used in the Experimental Earthscape Basin (XES) [*Sheets et al.*, 2002]. Unlike the XES system, however, where the topography of the entire fluvial surface is mapped periodically, topography was monitored at 2 min intervals along three flow-perpendicular transects, located 1.50 m, 1.75 m, and 2.00 m from the infeed point. To measure a full cross section of topography, including areas inundated by water, the experiment was stopped every 2 min and water was allowed to drain off the fluvial surface prior to collecting measurements. The time series of deposition along the transect located 1.75 m from the infeed is shown in Figure 2. With this system, we obtained measurements with a sampling interval of 0.8 mm in the horizontal and measurement pre-

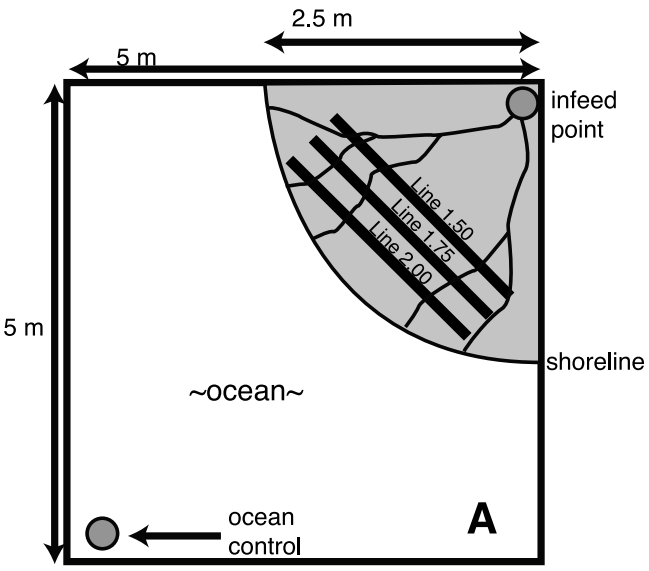

Figure 1. (a) Schematic of the experimental arrangement. The data used in this study are of the transect labeled Line 1.75. This transect is located at a perpendicular distance of 1.75 m from the sediment infeed point. (b) A photograph of the DB-03 experiment at a run time of approximately 11 h.

cision of 0.9 mm in the vertical. This experiment lasted for 30 h and produced an average of 15 cm of stratigraphy.

[10] No attempt was made to formally upscale the results from this experiment to field scale. In addition, parameters associated with this experiment were not set to produce an analog to any particular field fan-delta system. As such, specific geometric data associated with this experiment cannot strictly be utilized to estimate the field-scale deposit geometries or dynamics of a specific system. Rather, the goal of the experiment was to create a self-organized, distributary depositional system in which many of the processes characteristic of larger fan-delta systems could be monitored in detail over spatial and temporal scales which are impossible to obtain in the field. This experimental technique relies on similarity arguments advanced by *Hooke* [1968] and *Paola et al.* [2009]. As such the focus in this paper is on identifying the general class of distributions (i.e., heavy versus thin tail) which characterize the dynamics of topography in the DB-03 experiment and their relation to the architecture of the preserved stratigraphy.

3. Terminology

[11] The experimental data used in this study consist of a 30 h temporal evolution of an elevation transect (Line 1.75 in Figure 1a) with a temporal resolution of 2 min (as described in section 2). At any spatial location along the Line 1.75, we define elevation increments in time as

$$\delta h(t) = h(t + \Delta t) - h(t), \tag{1}$$

where $h(t)$ is the elevation at time t at a given location and Δt is the temporal resolution of the experimental data. Figure 3 shows the elevation increments at three different locations along Line 1.75. Positive values of elevation incre-

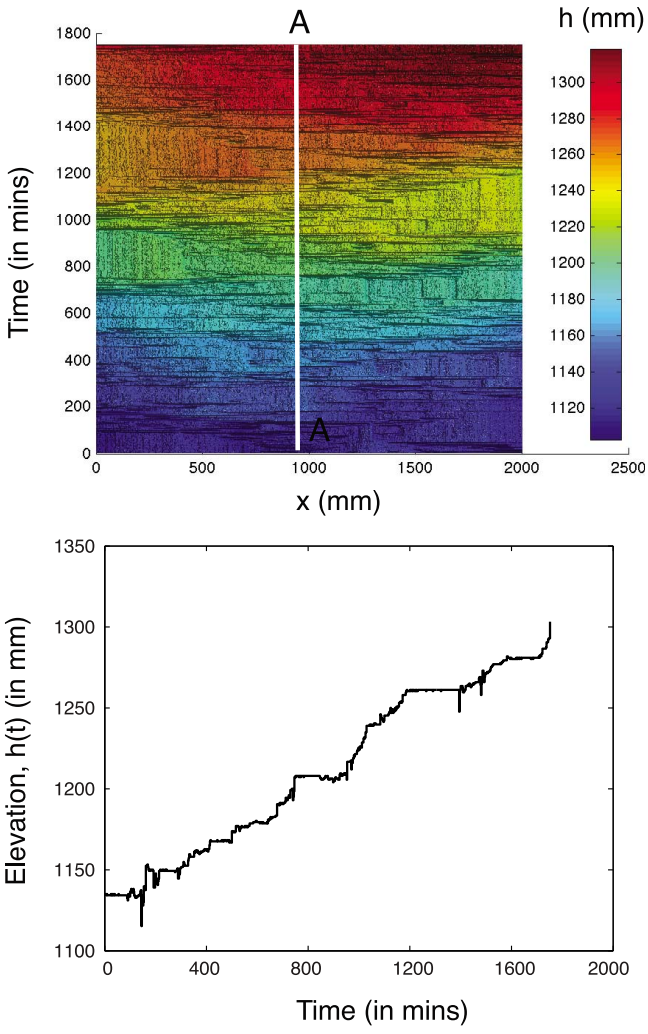

Figure 2. Temporal evolution of the transect Line 1.75. The temporal resolution of the data available is 2 min, and the duration for which the data was recorded is 30 h. (top) A time transect of elevation is marked as A-A; (bottom) the plot of that transect is shown.

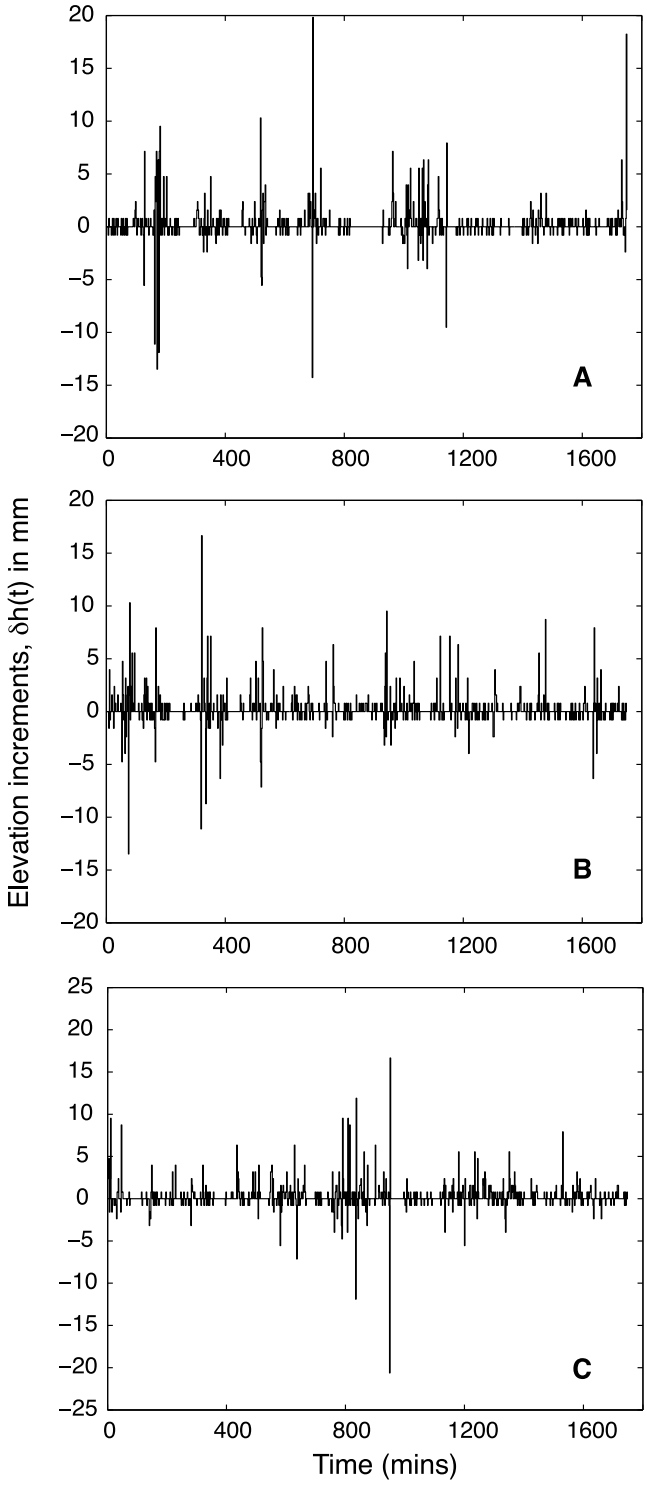

Figure 3. (a–c) Elevation increments in time along three different transects. Figure 3a corresponds to transect A-A in Figure 2. The positive values indicate magnitude of depositions, the negative values indicate magnitude of erosions, and the zero values indicate periods of inactivity.

ments correspond to deposition, negative values to erosion and were denoted as

$$D_i = \delta h(t) > 0 \tag{2a}$$

$$E_i = \delta h(t) < 0, \tag{2b}$$

respectively, while $\delta h(t) = 0$ corresponds to inactivity at that given location. Each of these three processes, deposition, erosion and inactivity, has a characteristic time scale of operation. Periods of inactivity, τ_i, are defined as continuous periods during which neither deposition nor erosion occurs in the system, that is, $\delta h(t) = 0$. Similarly, durations of depositional events, τ_d, are defined as the periods during which continuous deposition occurs in the system, that is, the uninterrupted periods for which $\delta h(t) > 0$, while durations of erosional events, τ_e, are defined as the periods during which continuous erosion occurs, the uninterrupted periods for which $\delta h(t) < 0$. Further, the magnitudes of a single depositional event (D_e) or an erosional event (E_e) are defined as the sum of all the elevation increments during the duration of a single depositional event (τ_d) or an erosional event (τ_e), respectively:

$$D_e = \sum_{i=1}^{\tau_d} D_i \tag{3a}$$

$$E_e = \sum_{i=1}^{\tau_e} E_i. \tag{3b}$$

It is easy to see that these magnitudes of depositional and erosional events are random sums of random variables. The schematic of Figure 4 shows the random variables defined which characterize the surface evolution of the depositional system. The statistical characteristics of this set of random variables ($\delta h(t)$, D_i, E_i, D_e, E_e, τ_d, τ_e, τ_i) are studied in section 4.

[12] The stratigraphic column that results from such an erosional-depositional process can be formed from the elevation time series as shown in the schematic of Figure 5. Stratigraphic deposits are depositional bodies bound between two erosional boundaries. The thickness of any deposit is denoted by D_{st}. The time interval demarcating the boundaries of the stratigraphic deposit D_{st} is denoted by τ_{st}. The

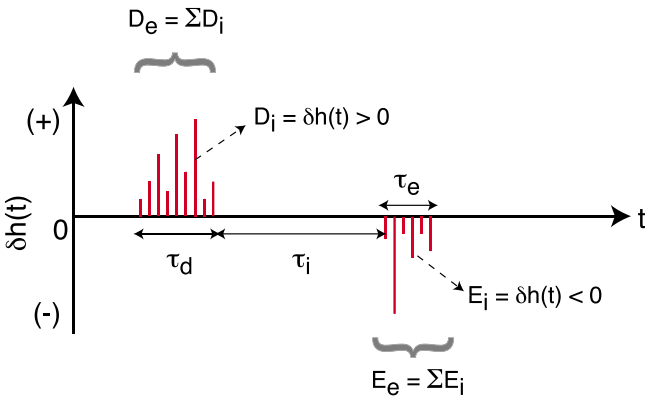

Figure 4. A schematic showing the elevation increments in time and the definitions of the random variables studied in section 4. Magnitudes and durations of erosional and depositional events, along with the periods of inactivity, are shown.

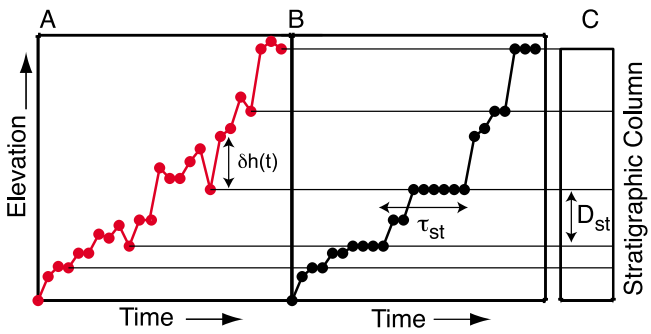

Figure 5. A schematic showing the building of a stratigraphic column from the elevation time series. Stratigraphic deposits are depositional bodies bound between two erosional events. Elevation increments ($\delta h(t)$), duration between stratigraphic deposits (τ_{st}), and thickness of stratigraphic deposits (D_{st}) are shown.

preserved stratigraphy is completely described by these two random variables (D_{st} and τ_{st}) whose statistical properties are studied in section 5.

4. Statistical Characteristics of Surface Evolution

[13] In this section, we present statistical analysis of random variables that govern the surface dynamics of delta evolution, namely, surface elevation increments (D_i, E_i), the magnitudes of erosional and depositional events (D_e, E_e) and durations of erosional and depositional events (τ_d, τ_e), as well as the periods of inactivity, τ_i. All the statistics presented in sections 4.1 and 4.2 were computed on the ensemble of time transects along the horizontal line (as shown in Figure 2) and the total number of time transects available was 2502, each for a duration of 30 h.

4.1. Statistics of Erosional and Depositional Magnitudes

[14] Consider the elevation increments, $\delta h(t)$, as defined in equation (1). Figure 6 shows the probability density function (pdf) of the elevation increments normalized by their standard deviation in semilog scale. It is noted that the pdf of increments exhibits a concave-up decay in the tails of the pdf indicating a heavy-tail behavior and considerably deviates from a Gaussian pdf (shown as the solid parabola in Figure 6). The log-log linear decay (see Figures 7a and 7c) in the left and right tails of the elevation increments establishes that the positive and negative increments (deposition and erosion, respectively) are heavy tailed. In contrast to thin-tailed pdfs, where the chance of occurrence of an extreme event is nearly zero, in heavy-tailed pdfs an extreme event has a small, but significant chance of occurrence. Heavy-tailed pdfs often have a power law decay, which is a slower decay than exponential (e.g., exponential pdf) and superexponential decays (e.g., Gaussian pdf), thus, assigning a relatively higher probability for the occurrence of extremes. In this section we characterize the pdfs of both erosional ($E_i = \delta h(t) < 0$) and depositional ($D_i = \delta h(t) > 0$) magnitudes.

[15] A common pdf with power law decay is a Pareto distribution. The density of a Pareto distribution is given by

$$f(x) = \alpha \frac{\gamma^{\alpha}}{x^{\alpha+1}}, \tag{4}$$

where α is the tail index, γ is the minimum possible value of the random variable and the density is defined for $x \geq \gamma$. The probability of exceedance of a Pareto distribution is given by

$$P(X > x) = \left(\frac{\gamma}{x}\right)^{\alpha}. \tag{5}$$

It is easy to see that a Pareto distribution assigns a finite probability for the occurrence of very large magnitude events (no upper limit), which do not typically occur in natural systems owing to constraints set by physical mechanisms that govern the evolution of the system (for example, see [*Bruno et al.*, 2004] and [*Zhang et al.*, 2007] for upper bounds reported on probability distributions of other systems). One common truncated heavy-tailed, power law pdf is the truncated Pareto distribution. The density of the truncated Pareto distribution is given by

$$f(x) = \frac{\alpha \gamma^{\alpha} x^{-\alpha-1}}{1 - (\gamma/\nu)^{\alpha}}, \tag{6}$$

and its probability of exceedance is given by

$$P(X > x) = \frac{\gamma^{\alpha}(x^{-\alpha} - \nu^{-\alpha})}{1 - (\gamma/\nu)^{\alpha}}, \tag{7}$$

where ν is the truncation parameter or the upper bound on the random variable, α is the tail index and γ is the lower bound on the random variable X. We fitted Pareto and truncated Pareto distributions to both the depositional

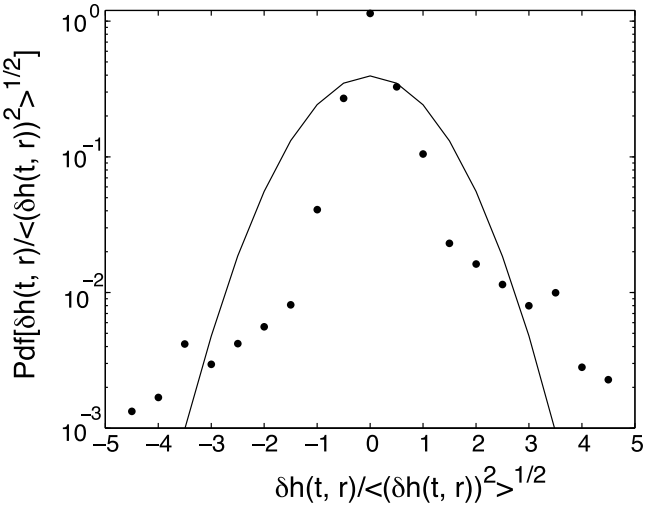

Figure 6. Relative frequency of elevation increments $\delta h(t)$ in semilog scale (solid circles); the solid line indicates a Gaussian density. The concave-up shape of the tails indicate the presence of heavy-tailed behavior (a linear decay corresponds to exponential decay of tails) and show that elevation increments deviate considerably from Gaussian behavior.

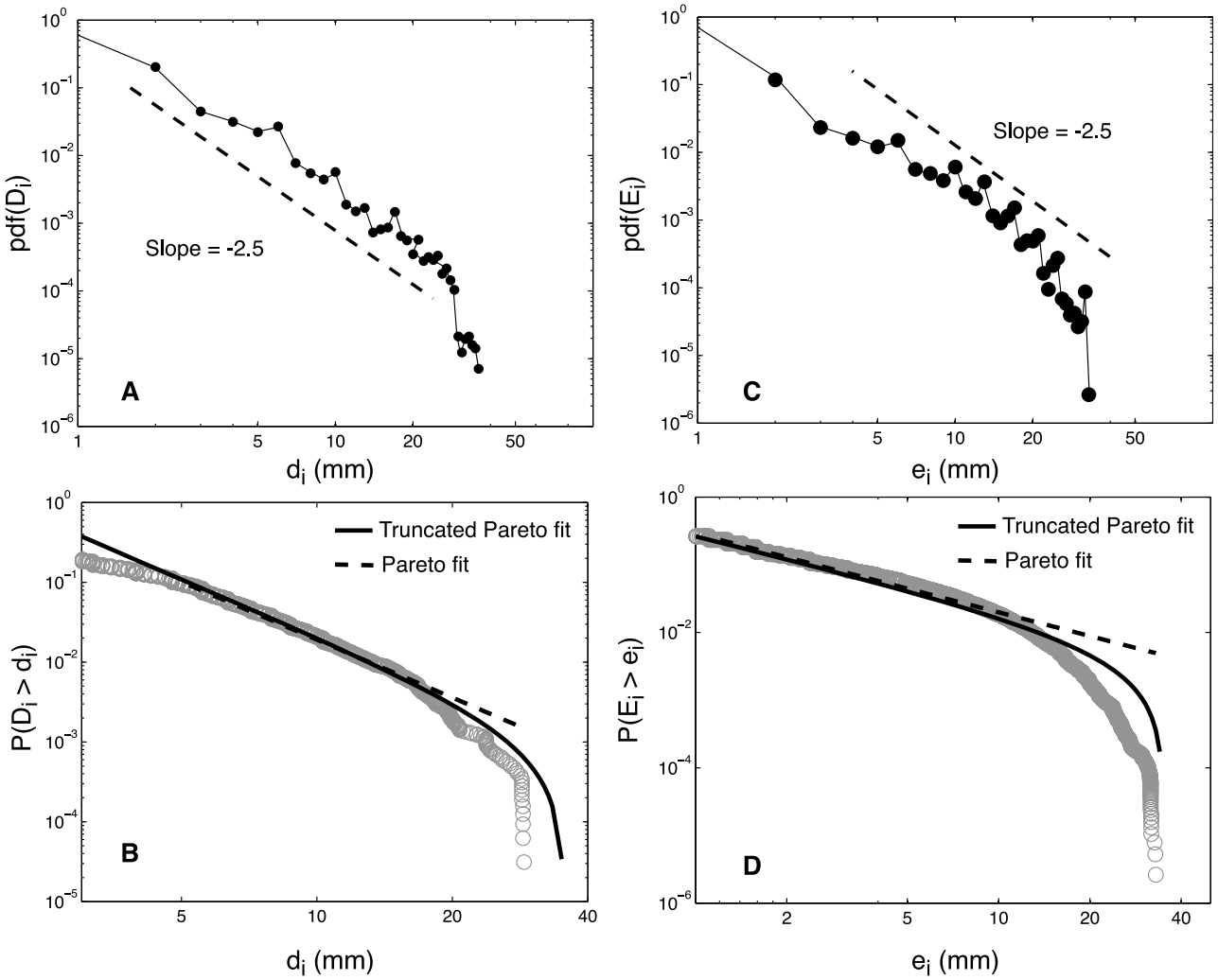

Figure 7. Log-log plot of probability density function of (a) positive elevation increments (D_i) and (c) negative elevation increments (E_i). An indicative slope of −2.5 is shown for reference to establish a power law decay of this distribution. Log-log plot of probability of exceedance for (b) positive elevation increments and (d) magnitudes of negative elevation increments (open circles) along with the best fit truncated Pareto distribution (solid black line) and best fit Pareto distribution (dashed line). The estimated parameters of these distributions are summarized in Table 1.

and erosional magnitudes, as shown in Figures 7b and 7d, respectively.

[16] In the work by *Clauset et al.* [2009], a maximum likelihood estimation (MLE) method was proposed to estimate the parameters α and γ of the Pareto distribution and that method is adopted in this study. In the work by *Aban et al.* [2006], a MLE method was proposed to estimate the parameters of the truncated Pareto distribution and this method is adopted in our study. The estimation involves the conditional MLE based on the $(k + 1)$ largest-order statistics representing only the portion of the tail where the truncated Pareto approximation holds. Let $X_1, X_2, \cdots, X_n$ denote a random sample from a truncated Pareto distribution, and $X_{(1)} \geq X_{(2)} \geq \cdots \geq X_{(n)}$ denote its order statistics, where $X_{(k)}$ is the kth largest observation. The conditional MLE for the parameters of the truncated Pareto distribution based on the $(k + 1)$ largest-order statistics is given by $\hat{\nu} = X_{(1)}$, $\hat{\gamma} = k^{1/\hat{\alpha}}(X_{(k+1)})\,[n - (n-k)(X_{(k+1)}/X_{(1)})^{\hat{\alpha}}]^{-1/\hat{\alpha}}$, and $\hat{\alpha}$ is obtained by solving

$$\frac{k}{\hat{\alpha}} + \frac{k\left(X_{(k+1)}/X_{(1)}\right)^{\hat{\alpha}} \ln\left(X_{(k+1)}/X_{(1)}\right)}{1 - \left(X_{(k+1)}/X_{(1)}\right)^{\hat{\alpha}}} - \sum_{i=1}^{k}\left[\ln X_{(i)} - \ln X_{(k+1)}\right] = 0. \tag{8}$$

Aban et al. [2006] proposed an asymptotic level-q test $(0 < q < 1)$ which rejects the null hypothesis $H_0{:}\nu = \infty$ (Pareto distribution) when $X_{(1)} < [(nC)/(-\ln q)]^{1/\alpha}$, where $C = \gamma^{\alpha}$. The corresponding p value of this test is given by $p = \exp(-nCX_{(1)}^{\alpha})$. In practice, they proposed the use of the Hill's estimator,

$$\hat{\alpha}_H = \left(k^{-1}\sum_{i=1}^{k}\left(\ln X_{(i)} - \ln X_{(k+1)}\right)\right)^{-1} \tag{9a}$$

Table 1. Estimated Parameters of Fitted Truncated Pareto and Pareto Distributions[a]

		Truncated Pareto Fit			Pareto Fit	
Random Variable	Sample Size	Tail Index	Upper Bound	Lower Bound	Lower Bound	Tail Index
D_i (mm)	565,237	2.41	35	2	5.2	2.41
E_i (mm)	379,931	1.1	35	0.3	1.2	1.16
D_e (mm)	76,220	3.31	40	4.5	12.5	3.31
E_e (mm)	52,064	3.03	25	2.7	9.5	3.03
τ_i (min)	186,172	1.14	240	8	84	2.44
τ_{st} (min)	133,888	0.7	320	4	10	0.88

[a]The standard error of estimate for the all parameters is of the order of 10^{-3} in view of the large sample size.

$$\hat{C} = \frac{k}{n}\left(X_{(k+1)}\right)^{\hat{\alpha}_H} \tag{9b}$$

for the estimation of parameters C and α. A small value of $p < 0.1$ (suggested by *Clauset et al.* [2009] as a conservative estimate) in this case indicates that the Pareto distribution does not provide a good fit to the data. A detailed description of the proofs and method for estimating the parameters of the distribution can be found in the work by *Aban et al.* [2006].

[17] Using the above test, we rejected the Pareto distribution for D_i and E_i as the estimated p values (0.0022 and 0.0048) were less than 0.1. However, the truncated Pareto distributions provided an acceptable fit to the data for the magnitudes of D_i and E_i (see Figure 7). The estimated tail indices of the best fit truncated Pareto distributions for positive elevation increments, D_i, and negative elevation increments, E_i, are $\hat{\alpha}_1 = 2.41$ and $\hat{\alpha}_2 = 1.1$, respectively (see Table 1 for a summary of the parameters of the fitted distributions and the lengths of the series available for computing the statistics). *Aban et al.* [2006] suggested that goodness of fit of the truncated Pareto distribution is a graphical check of the data tail. The upper bound on both these pdfs was found to be 35 mm. These findings lend strong support for the use of heavy-tailed distributions for the modeling of dynamics of surface evolution in this deltaic system.

[18] Further, we defined the magnitude of a depositional event as the sum of the elevation increments over the duration of that deposition (equation (3a)). These random sums of elevation increments are the thickness of a stratum before any further erosion occurs, as defined by *Kolmogorov* [1951]. Erosional events were defined as the random sum of magnitudes of negative increments over the duration of erosional events. It is important to note that the depositional and erosional events are the random variables which finally define the thickness of the preserved stratigraphic column [*Kolmogorov*, 1951]. Figure 8 shows the probability of exceedance of D_e and E_e along with their best fit Pareto and truncated Pareto distributions. The Pareto distribution does not provide a good fit to the data of D_e and E_e and the estimated p values of the fits were 4.05×10^{-4} and 1.63×10^{-6}, respectively. The tail indices of the best fit truncated Pareto distributions for D_e and E_e are $\hat{\alpha}'_1 = 3.31$ and $\hat{\alpha}'_2 = 3.03$, respectively. The distributions of the depositional and erosional events have a faster decay of tails than their parent distributions of D_i and E_i ($\hat{\alpha}'_1 > \hat{\alpha}_1$ and $\hat{\alpha}'_2 > \hat{\alpha}_2$), indicating that heavy-tailed surface statistics need not always be preserved in the stratigraphic column thicknesses as the random variables which govern the thickness of deposits have thinner tails than their parent distributions. In section 4.2, we present the analysis of the time statistics of surface evolution, that is, the durations of erosional and depositional events and periods of inactivity.

4.2. Statistics of Periods of Inactivity

[19] The relative frequencies computed from the experimental data of the durations of depositional and erosional events, as well as the periods of inactivity, are shown in Figures 9a, 9b, and 9c, respectively. It was found that the mean and standard deviations of the durations of depositional

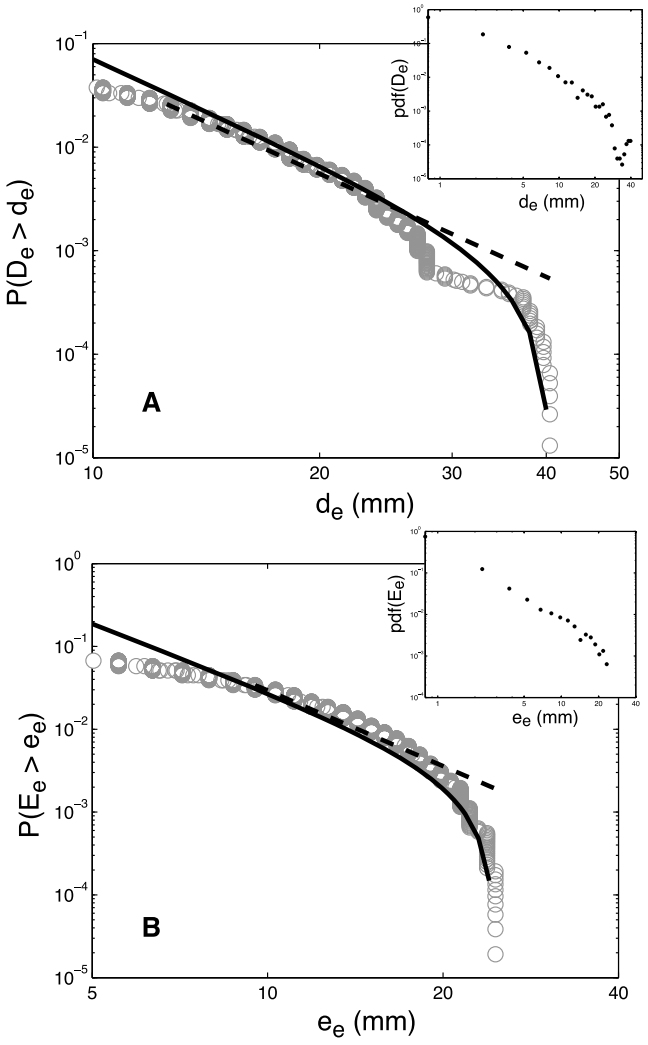

Figure 8. Log-log plot of probability of exceedance of (a) depositional events (D_e) and (b) erosional events (E_e). The insets show the log-log plots of the probability density functions of depositional and erosional events. Best fit truncated Pareto distributions are shown in solid black lines, and the best fit Pareto distributions are shown in dashed lines. Note that in both cases a random sum of the elevation increments results in a distribution with a thinner tail than the parent distribution (see Table 1 for estimated parameters).

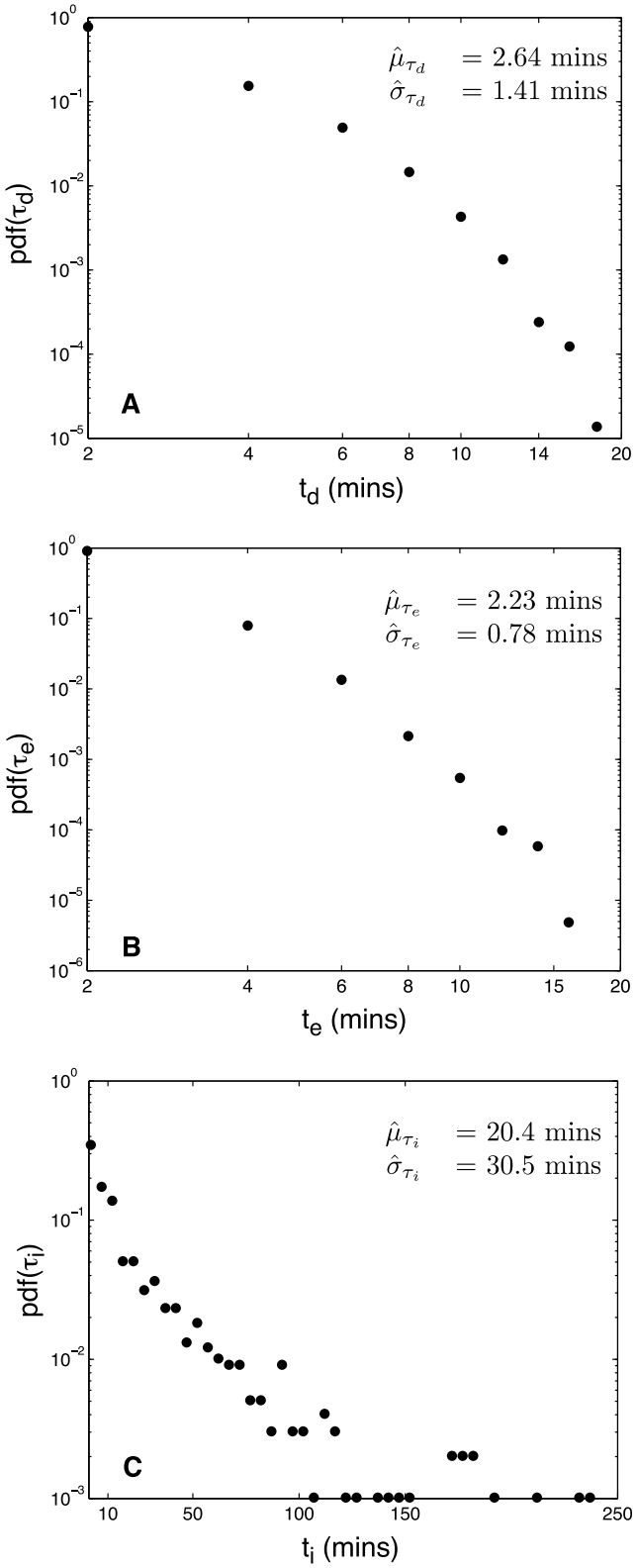

Figure 9. Probability density functions of (a) the duration of depositional events (τ_d), (b) the duration of erosional events (τ_e) on a log-log plot, and (c) the periods of inactivity (τ_i) on a semilog plot. The bin size has been selected equal to 2 min, which is the temporal resolution of the series. It is noted that the dominant time scale in the system is that of inactivity.

and erosional events were $\hat{\mu}_{\tau d}$ = 2.64 min, $\hat{\sigma}_{\tau d}$ = 1.41 min and $\hat{\mu}_{\tau e}$ = 2.23 min, $\hat{\sigma}_{\tau e}$ = 0.781 min, respectively, while the mean and standard deviation of the periods of inactivity were $\hat{\mu}_{\tau i}$ = 20.4 min and $\hat{\sigma}_{\tau i}$ = 30.52 min. It is noted that the mean and standard deviations of τ_d and τ_e are an order of magnitude less than that of τ_i, indicating that the dominant temporal scale of the system is that of inactivity. The durations of erosion and deposition events have a mean approximately equal to the temporal resolution of the data with a very small standard deviation and it was found that an exponential distribution adequately describes these random variables.

[20] The periods of inactivity, τ_i, were found to have a heavy-tailed distribution characterized by a log-log linear decay of pdf as shown in inset plot of Figure 10. Figure 10 shows the probability of exceedance and the best fit Pareto and truncated Pareto distributions to the data of periods of inactivity. The Pareto distribution does not provide a good fit to the data of periods of inactivity and the estimated p value of the fit was 0.056. The truncated Pareto distribution (equation (7)), fitted using the method proposed by *Aban et al.* [2006] (which is briefly outlined in section 4.1), was found to provide a good fit to the experimental data. The parameters of the fitted distribution were tail index, $\hat{\beta}$ = 1.14, lower bound, $\hat{\gamma}$ = 8 min and upper bound, $\hat{\nu}$ = 240 min. The truncation parameter $\hat{\nu}$ is equal to 4 h and is expected to be governed by some physical forcing (autogenic dynamics) of the depositional system, and specifically to the character-

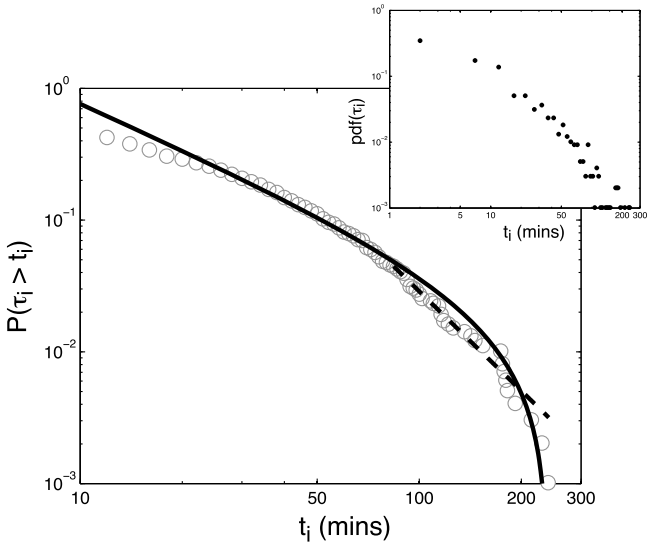

Figure 10. Probability of exceedance plot of the periods of inactivity τ_i plotted on a log-log scale. The open circles indicate the empirical density of the data, the thick solid line shows the best fit truncated Pareto distribution, and the dashed line shows the best fit Pareto distribution. The parameters of the truncated Pareto distribution are tail index $\hat{\beta}$ = 1.14 and truncation parameter $\hat{\nu}$ = 240 (4 h). The truncation parameter $\hat{\nu}$ was found to correspond to the avulsion time scale of the mean channel depth, which is around 2 cm in the system. The inset plot shows the pdf of τ_i on a log-log scale. Notice the power law decay of the distribution, indicating a heavy-tailed behavior.

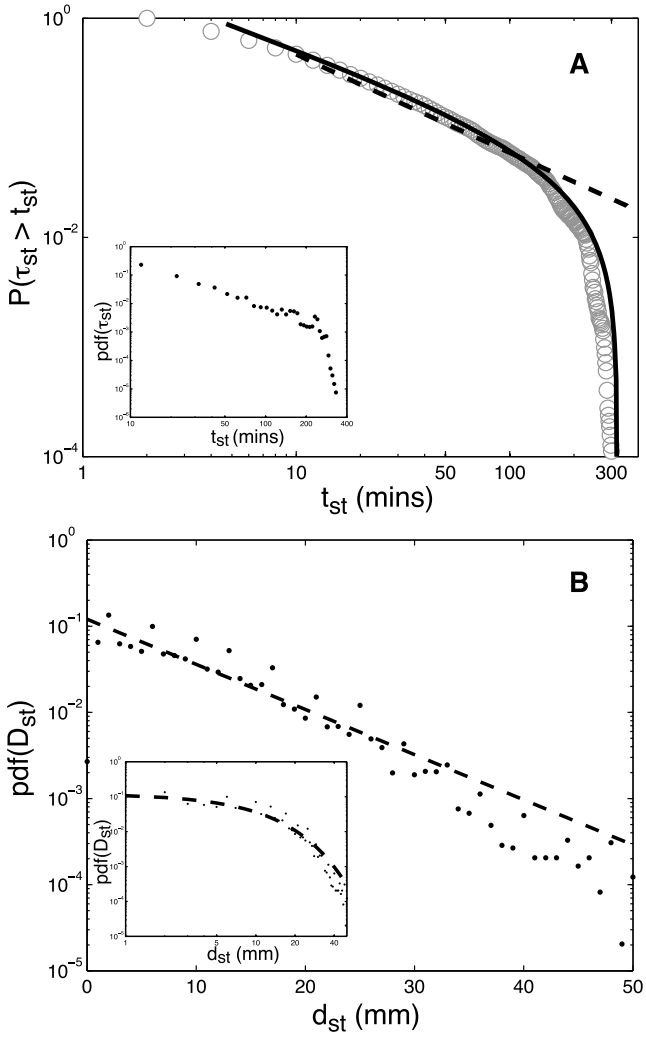

Figure 11. (a) Probability of exceedance of the time interval demarcating the stratigraphic deposit (τ_{st}), along with its best fit truncated Pareto (solid line) and Pareto distributions (dashed line). The inset plot shows the pdf of τ_{st} on a log-log scale. (b) Semilog plot of the pdf of bed thickness (D_{st}) along with the best fit exponential distribution (dashed line). The estimated mean of the fitted exponential distribution is 8.3 mm. The inset figure shows the exponential fit on a log-log scale.

istic avulsion time scale of the channels, as will be discussed in section 7. Thus, we conclude that the random variables which govern the dynamics of surface evolution, namely, D_i, E_i, D_e, E_e, and τ_i, all exhibit heavy-tailed statistics.

5. Statistics of Preserved Stratigraphy

[21] Stratigraphic columns can be built from the elevation time series (see Figure 5) and in this section we analyze the statistics of the stratigraphic deposit thickness (D_{st}) and the time interval demarcating the boundaries of the stratigraphic deposits, τ_{st} (called "hiatuses" by *Schumer and Jerolmack* [2009]).

[22] The inset plot of Figure 11a shows the pdf of the time interval demarcating the stratigraphic column in a log-log plot. It is noted that τ_{st} shows a heavy-tailed behavior which can be seen from the power law decay of the pdf. Figure 11a shows the probability of exceedance of τ_{st} along with its best fit Pareto and truncated Pareto distributions (see Table 1 for a summary of estimated parameters of these distributions). The Pareto distribution does not provide a good fit to the data of τ_{st} and the estimated p value from equation (9) was found to be 0.0017. The truncated Pareto distribution provides a better fit than the Pareto distribution to the experimental data with estimated parameters: tail index $\hat{\beta}' = 0.7$, upper bound $\hat{\nu}' = 320$ min, and a lower bound 10 min. The time interval demarcating the stratigraphic deposits is a random sum of durations of erosional and depositional events (τ_d and τ_e) as well as the periods of inactivity (τ_i). Since the dominant time scale is given by the periods of inactivity, τ_{st} is in effect a random sum of the periods of inactivity. The tail index of τ_{st} is lower, $\hat{\beta}' = 0.7$, indicating a heavier tail for τ_{st} than its parent distribution of τ_i ($\hat{\beta} = 1.1$). The implications of the tail index of τ_{st} being less than 1 and the mechanisms that set the scales of truncation on this pdf are discussed in section 7.

[23] Further, we analyze the statistics of the bed thickness of preserved stratigraphic columns (D_{st}) to characterize the nature of the pdf of the thickness of the preserved stratigraphic columns. As shown in Figure 11b, an exponential distribution provides a good fit to the recorded bed thickness. The estimated mean of the exponential distribution is 8.3 mm. It is interesting to note that although the surface evolution is governed by heavy-tailed statistics of erosion and deposition, the preserved bed thickness does not carry a signature of these heavy-tailed statistics. This was also documented via numerical simulations by *Straub et al.* [2010]. In section 6, we characterize the self-similar fractal structure of the temporal evolution of the surface elevations.

6. Multifractality of Surface Evolution

[24] Surface elevation increments are found to exhibit variability at all scales. For example, Figure 12 shows the temporal evolution of a given transect (transect A-A in Figure 2) that possesses a Devil's staircase–like structure. Notice that visually, the structure of evolution when viewed at different time scales (shown as inset plots in Figure 12) looks statistically similar. One common way of documenting the self-similar structure of a given time series is to look at the power spectral density of the time series. Figure 13 shows the power spectral density as a function of wavelength for the ensemble of temporal transects along Line 1.75. A power law decay, with an exponent of $\phi = -2.1$ documents the presence of statistical scaling in the temporal evolution of elevation time series. The Hurst exponent (H) which is a measure of the "roughness" of the time series is related to the spectral density's power law decay exponent as $-\phi = 2H + 1$ [*Turcotte*, 1992] resulting thus in $H = 0.55$. The fractal dimension D_0 and the Hurst exponent relate as $D_0 = 2 - H$ [e.g., *Turcotte*, 1992], leading to an estimated fractal dimension for the elevation time series of $D_0 = 1.49$.

[25] The power spectral density expresses the scaling of the second-order moment (variance) of the series and completely characterizes the scaling of Gaussian random vari-

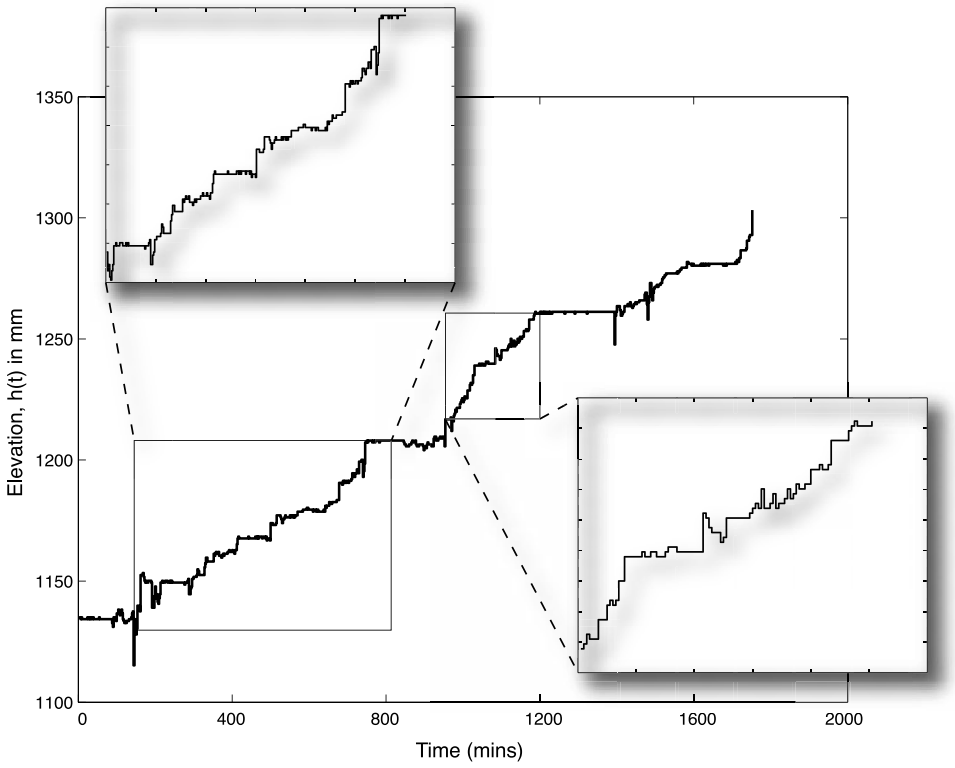

Figure 12. Time transect of elevation surface (A-A transect in Figure 2). The Devil's staircase–like structure is shown in the plot by magnifying small portions of the elevation transect over time. The flat periods in the top inset plot show the periods of inactivity in the system.

ables. Since the pdf of elevation increments was documented to significantly deviate from the Gaussian form, it is important to test for scaling in higher-order statistical moments. We performed higher-order structure function analysis of the elevation time series to characterize the statistical scaling of the temporal evolution of the deltaic surface. Elevation increments in time were computed at different scales r, denoted by $\delta h(t, r)$, as

$$\delta h(t,r) = h(t + r\Delta t) - h(t), \tag{10}$$

where Δt is the temporal resolution of the experimental data. The estimates of the qth-order statistical moments of the absolute values of elevation increments at scale r, also called structure functions, $M(q, r)$, are defined as

$$M(q,r) = \frac{1}{N_r}\sum_{t=1}^{N_r}|\delta h(t,r)|^q, \tag{11}$$

where N_r is the number of data points of elevation increments at a scale r. Statistical scaling, or scale invariance, requires that $M(q, r)$ be a power law function of the scale

$$M(q,r) \sim r^{\zeta(q)}, \tag{12}$$

where $\zeta(q)$ is the scaling exponent function. When the scaling exponent function has a linear dependence on the

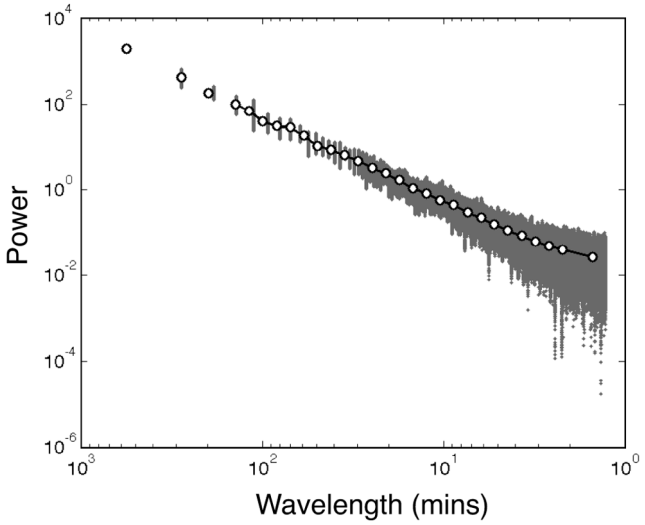

Figure 13. Power spectral density of elevation time transects on a log-log plot. The gray dots correspond to the power spectral density of each of the time transects, and the solid white circles indicate the log-binned average of the power spectral density. The log-log linear decay with an exponent of $\phi = -2.1$ establishes the self-similar structure of the elevation time series.

order of the statistical moments, that is, $\zeta(q) = qH$, the series is called monofractal and H is the Hurst exponent discussed previously. If the scaling exponent function has a nonlinear dependence on the order of statistical moments then the series is called a multifractal. The simplest way to characterize the nonlinear dependence of $\zeta(q)$ on q is by using a quadratic approximation,

$$\zeta(q) = c_1 q - \frac{c_2}{2} q^2, \tag{13}$$

where c_1 and c_2 are constants parameterizing the scale invariance of the series over a range of scales [see *Arneodo et al.*, 1998; *Venugopal et al.*, 2006]. Note that from equation (11) the zero-order structure function $M(0, r)$ is trivially equal to 1 and thus (from equation (12)) scale-independent. This approach therefore, does not allow us to characterize the possible fractality of the "sparseness" of the data series. However, as seen in section 4.2, the periods of inactivity exhibit a heavy-tailed distribution implying the existence of flat regions of all scales in the evolution of the elevation time series (see Figure 12) or sequences of zeroes of all scales in the time series of elevation increments (see Figure 3). Quantifying the nontrivial scaling of the zeroth-order moment of a data series would require relaxing the $\zeta(0) = 0$ assumption in equation (13) and introducing a positive constant c_0 in the characterization of the nonlinear dependence of the scaling exponents,

$$\zeta(q) = c_0 + c_1 q - \frac{c_2}{2} q^2 \tag{14}$$

Figure 14a shows the estimated higher-order structure functions, $M(q, r)$, as a function of scale r. The log-log linear relationship of $M(q, r)$ on r over the range of scales 2–256 min (2^1–2^8 in log scale) for the moments of order q = 0.1, 0.25, 0.5, 0.75, 1.0,…, 3.0 documents the scale invariance of the elevation increments. In Figure 14b, the scaling exponent function $\zeta(q)$ is plotted against the order of moments. The nonlinear dependence of $\zeta(q)$ on q documents the multifractal behavior of the elevation increments. Fitting the quadratic function of equation (14) to $\zeta(q)$ results in $c_0 = 0.192$, $c_1 = 0.58$ and $c_2 = 0.171$. These three parameters c_0, c_1 and c_2 fully characterize the scaling of all statistical moments and thus the way the pdfs of elevation increments change over scales [e.g., see *Venugopal et al.*, 2006].

[26] The analysis presented above provides a way of quantifying the multifractality of a signal via the scaling of its statistical moments. This statistical approach admits an interesting geometrical interpretation in terms of characterizing the "roughness" of a signal or its local singularity (degree of differentiability). A quantitative measure of local singularity is given by the so-called Hölder exponent $\mathcal{H}$ (see

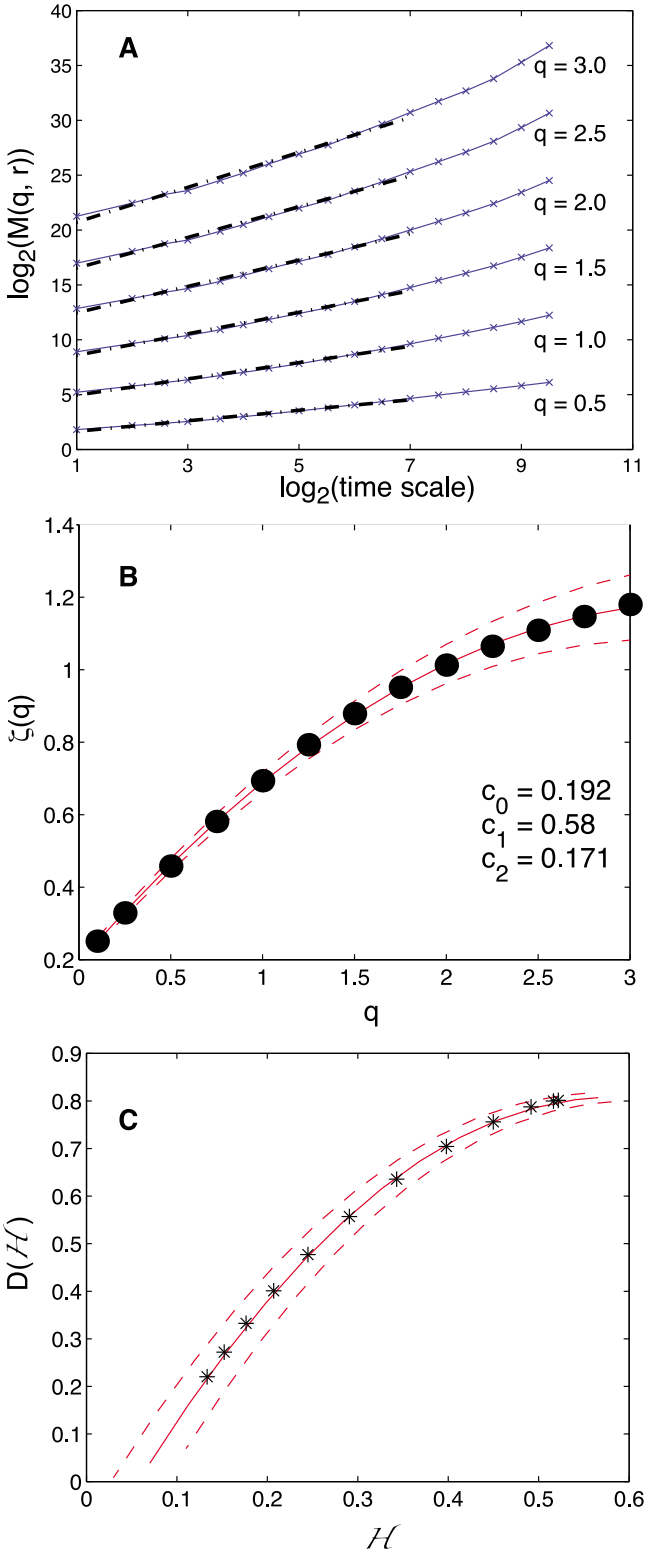

Figure 14. (a) Log-log plots of higher-order structure functions $M(q, r)$ versus r. The power law dependence documents the presence of scale invariance in the elevation time series $h(t)$. (b) The dependence of scaling exponent function, $\zeta(q)$, on the order of moments. The nonlinear dependence documents the presence of multifractal behavior with $c_0 \approx 0.192$, $c_1 \approx 0.58$ (the most prevailing Hurst exponent in the series), and $c_2 \approx 0.171$ (intermittency parameter). (c) Spectrum of Hölder exponents calculated from the scaling exponent function using equation (A4). The spread indicates the variability in the singularity exponents found in the elevation time series.

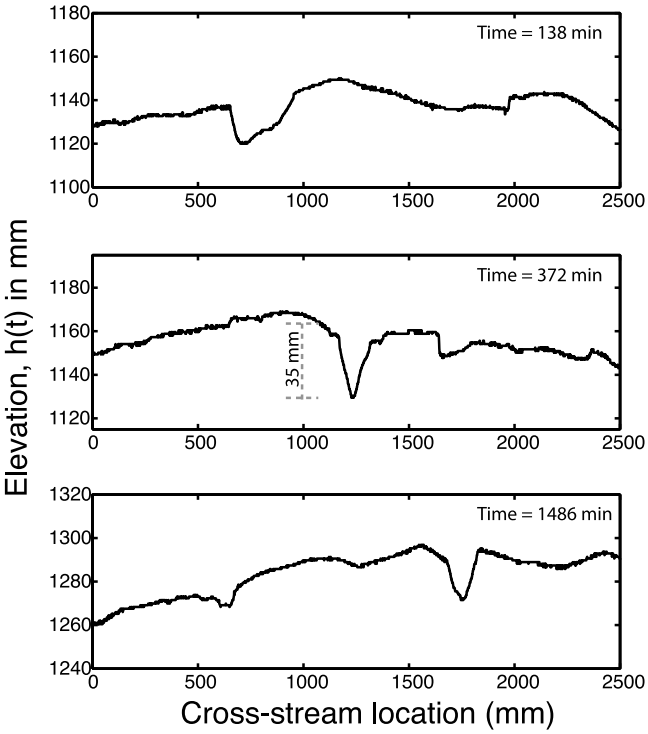

Figure 15. (top, middle, bottom) Elevation cross sections showing the deepest channels in the system at three different time steps during the experimental run. The 35 mm deep channel highlighted in Figure 15 (middle) was the deepest channel that appeared during the experimental run.

equation (A1) in Appendix A). When more than one singularity is present in the signal, the spectrum of singularities $D(\mathcal{H})$ quantifies the range of singularities and the fractal (Hausdorff) dimension of the support of these singularities. This spectrum of singularities $D(\mathcal{H})$ directly relates to the scaling exponent function $\zeta(q)$ via a Legendre transform (see Appendix A).

[27] Figure 14c shows the estimated $D(\mathcal{H})$ curve for surface elevation increments. Several observations are made from Figure 14c. First, the most prevailing singularity (peak of the D($\mathcal{H}$) curve) is equal to $\langle\mathcal{H}\rangle = 0.55$, which is almost identical to the single Hurst exponent computed from the power spectral analysis. Second, the $D(\mathcal{H})$ curve indicates the presence of a wide spectrum of singularities from 0.1 to 0.9 (the spectrum of Figure 14c is the left part of the full spectrum and due to the quadratic form of $\zeta(q)$ the spectrum is symmetrical around the mean value of $\langle\mathcal{H}\rangle$). Recall that regions in the elevation series where $\mathcal{H} \approx 0.1$ correspond to regions of abrupt changes in elevation series (large spikes in elevation increments in Figure 3) while $\mathcal{H} \approx 0.9$ corresponds to regions of a gradual change in the elevation series (smaller spikes in elevation increments). These spikes (local singularities) are interwoven in the signal and $D(\mathcal{H})$ characterizes their distribution. Third, it is observed that the fractal dimension of the most prevailing singularity is $D(\langle\mathcal{H}\rangle) = 0.8$ implying a sparseness in the surface elevation series consistent with the presence of periods of inactivity and the nonzero estimated value of c_0 in equation (14).

[28] As a final remark, we note that the scaling characterization presented above (via statistical moments or singularity spectrum) holds within a range of scales (see Figure 14a) whose upper bound coincides with the truncation parameter of the dominant time scale of the system, that is, periods of inactivity ($\hat{\nu}$ = 240 min), providing thus a much desired physical interpretation of the upper bound of the scaling regime.

7. Channel Depths as a First-Order Control on Depositional Systems

[29] In this section, we interpret the results on the truncation scales of the fitted distributions to the random variables that govern the surface evolution of depositional systems and show that channel depths act as a first-order control in setting the truncation scales (see Table 1 for a summary of parameters of fitted distributions). The observed mean channel depth in the DB-03 experiment was reported to be of the order of 2 cm, while the maximum channel depth was reported to be about 3 cm [*Sheets et al.*, 2007]. Specifically, the maximum channel depth calculated from the topographic cross sections (see Figure 15) was 35 mm, which is equal to the estimated upper bound of both the magnitudes of erosion and deposition (E_i and D_i). This indicates that the maximum channel depth acts as a first-order control on the truncation scale of pdfs of D_i and E_i. Physically, the maximum amount of deposition is governed by the maximum accommodation space available, which in this experiment corresponds to the maximum channel depths. Thus, we note that the maximum channel depths of the actively deforming surface provide an indicative measure of the truncation parameter or the upper bound on the pdfs of D_i and E_i.

[30] The time statistics are expected to be governed by the time scale of avulsion of the channels in the depositional systems. *Mohrig et al.* [2000] define the characteristic avulsion time scale T_A in a depositional system as

$$T_A = \frac{\eta}{\sigma_A}, \tag{15}$$

where η is the average depth of the channels and σ_A is the vertical aggradation rate in the system. Substituting $\eta = 2$ cm and σ_A = 5 mm/h [*Sheets et al.*, 2007], one can easily see that the time scale that sets the scale of truncation of τ_i ($\hat{\nu}_i$ = 240 min) is roughly governed by the mean avulsion rate T_A. One way to think about this result is to consider the processes that set the periods of inactivity in a depositional system. The smaller values of τ_i arise in the system when that given location is occupied by a channel that is not depositing or eroding sediment. However, longer periods of inactivity arise from abandoning of a previously occupied channel location which leads to long periods of neither deposition nor erosion happening at that location. Indeed, the results from the best fit truncated Pareto distribution to the data of τ_i suggest that the larger values of τ_i have an upper bound which is governed by the mean avulsion rate of the system. However, in real systems this upper bound can be greater than the time scales of avulsion of the mean channel depths owing to climatic/environmental forcing, as the statistics of the experiment only reflect the autogenic effects on the

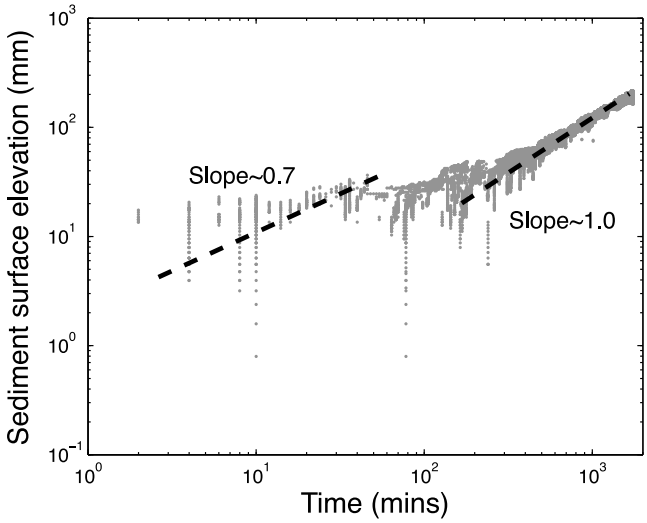

Figure 16. Plot showing the sediment surface elevation of the recorded bed thickness as a function of time on log-log scale. The scaling of the sediment surface elevation shows the effect of heavy-tailed "hiatuses" with a slope of $\beta' = 0.7$ until around the time scale of truncation of pdf of τ_{st}. For times larger than the scale of truncation, the sediment surface elevation scales linearly with time. The plot, when normalized with the time scales of observation, leads to the estimated deposition rate dependence on time (Sadler effect).

periods of inactivity. It is also interesting to note that *Straub et al.* [2009] show that channel depths act as a first-order control on the stratigraphic architecture of channelized sediment transport systems. *Straub et al.* [2009] found that the degree of compensation present in alluvial basins scales with the depths of the channels constructing the stratigraphy. Taken together, our study and the study of *Straub et al.* [2009] illustrate that channel depth is a fundamental length scale for both the surface dynamics of deltas and the architecture of deltaic stratigraphy.

[31] The time interval demarcating the stratigraphic deposits was documented to have a truncated Pareto distribution (see section 5). The best fit truncation parameter was found to be $\hat{\nu}' = 320$ min with a tail index of $\hat{\beta}' = 0.7$. The time scale of truncation corresponds to the avulsion time scale of a 2.7 cm deep channel (using equation (15)), which corresponds roughly to the deepest channels encountered during the experimental run. A heavy-tailed distribution for τ_{st} with a tail index less than 1, introduces a bias into the estimated deposition rates and leads to the so-called "Sadler" effect [*Sadler*, 1981; *Schumer and Jerolmack*, 2009]. Figure 16 shows the growth of the sediment surface elevation of the stratigraphic column with respect to time. As discussed by *Schumer and Jerolmack* [2009], the heavy-tailed behavior of "hiatuses" or the time interval demarcating the stratigraphic columns causes a sublinear growth of the sediment surface elevation for time scales less than the truncation in the pdf of τ_{st} with the scaling exponent equal to the tail index of τ_{st} ($\hat{\beta}' = 0.7$). For time scales larger than $\hat{\nu}'$, the sediment surface elevation grows linearly in time, indicating that there is no bias in the estimated deposition rates. Normalizing the sediment surface elevation increments with the time scale at which the process is observed leads to the estimated depositional rates' dependence on time. It is easy to see that the scaling of the observed deposition rates depends on the tail index of the distribution of τ_{st}, where the estimated deposition rates decay with a power law exponent of $\hat{\beta}' - 1 = -0.3$ until the time scale of truncation of τ_{st} and beyond the truncation scale $\hat{\nu}'$, the estimated deposition rates do not depend on the time scale of observation. Our experimental data confirm the hypothesis of *Schumer and Jerolmack* [2009] that the bias in estimated deposition rates does indeed arise from heavy-tailed "hiatuses." In the case when the heavy-tailed hiatuses (τ_{st}) arise from heavy-tailed periods of inactivity (τ_i), our analysis shows that the degree of bias in the estimated deposition rates (which can be calculated by the degree to which sediment surface elevation deviates from linear growth) can lead to the estimation of the tail index of the hiatuses. Moreover, the truncation scale of the pdf of hiatuses can be estimated from the avulsion time scale of the deepest channel in the system.

[32] The scaling regime of the multifractal behavior reported in section 6 was from 2 min to 256 min. The lower bound on this scaling regime corresponds to the temporal resolution of the data collected while the upper bound on this regime corresponds to the truncation parameter of the periods of inactivity (τ_i). This indicates that the scaling regime of the surface elevation time series can be derived from the physical controls of the system as the upper bound on the scaling regime is set by the time scale of avulsion of the mean channel depth.

8. Modeling of Surface Evolution and Sediment Surface Elevation of Stratigraphic Column

[33] In this section, we present some preliminary thoughts on modeling depositional systems using continuum models which are consistent with the heavy-tailed statistics documented in sections 4, 5, and 7. Recently, modeling Earth surface processes that possess variability over a large range of space time scales and exhibit heavy-tailed statistics has received considerable attention [e.g., *Stark et al.*, 2009; *Ganti et al.*, 2009, 2010; *Foufoula-Georgiou et al.*, 2010; *Schumer et al.*, 2009; *Foufoula-Georgiou and Stark*, 2010; *Bradley et al.*, 2010; *Harman et al.*, 2010]. In a recent study, *Voller and Paola* [2010] acknowledged the deviation of fluvial profiles from ones predicted by classical diffusion and proposed the exploration of fractional diffusive model to describe the observed steady state fluvial profiles in a depositional system. However, it is important to note that the underlying assumption of the fractional diffusive model is that the transport distances of sediment particles along the flow paths in depositional systems is heavy tailed (see *Ganti et al.* [2010], *Bradley et al.* [2010], and *Foufoula-Georgiou et al.* [2010] where the heavy-tailed nature of sediment transport distances are shown to result in a fractional diffusive model), for which we do not have direct experimental evidence. However, our results do indicate that the periods of inactivity are heavy tailed and this needs to be taken into account while modeling the surface dynamics of depositional systems.

[34] The classical diffusion equation has been used to model the surface dynamics of depositional systems [*Paola et al.*, 1992; *Paola and Voller*, 2005; *Pelletier and Turcotte*,

1997]. The underlying assumptions of the classical diffusion equation are thin-tailed periods of inactivity and thin-tailed transport distances for sediment particles and the governing equation for the elevation evolution at any point is given by [e.g., *Meerschaert et al.*, 1999]

$$\frac{\partial h}{\partial t} = D\frac{\partial^2 h}{\partial x^2} - \sigma_A, \tag{16}$$

where h is the surface elevation, D is the diffusivity coefficient, σ_A is the net aggradation rate and x is the distance along a flow path. A pure power law, heavy-tailed pdf for the periods of inactivity without any truncation leads to a time-fractional diffusion equation which describes the evolution of surface elevation in time [*Schumer et al.*, 2003; *Meerschaert and Scheffler*, 2004]. However, our experimental results indicate that the periods of inactivity are heavy tailed with an upper bound equal to the avulsion time scale of the mean channel depth. Truncated power law pdfs of periods of inactivity can be modeled using "tempered anomalous diffusion" equations where the power law pdf of periods of inactivity is described by tempered stable pdfs [*Meerschaert et al.*, 2008]. Tempered stable pdfs were proposed by *Cartea and del-Castillo-Negrete* [2007] and *Rosiński* [2007] as a smoother alternative to the truncated heavy-tailed pdfs which have a sharp cutoff. In this case, the truncation is not assumed to be a fixed threshold but is assigned an exponential tempering of rate λ where the pdf has a power law decay till a particular value and beyond that given truncation value the pdf decays exponentially. Assuming tempered stable pdfs of periods of inactivity and thin-tailed pdfs of transport distances of sediment particles, the governing equation that describes the evolution of the surface elevation can be shown [*Meerschaert et al.*, 2008] to be given by

$$\frac{\partial h}{\partial t} + e^{-\lambda t}\frac{\partial^\beta}{\partial t^\beta}\left(e^{\lambda t}h\right) - \lambda^\beta h = D\frac{\partial^2 h}{\partial x^2} - \sigma_A, \tag{17}$$

where x is the distance along the flow path, $\beta < 1$ is the tail index of periods of inactivity, D is diffusivity and λ is the rate of exponential tempering. The rate of exponential tempering, λ, is equal to the inverse of the mean of the truncation parameter, which is governed by the avulsion time scale of the mean channel depth in systems whose dynamics are set by purely autogenic processes (like the experimental arrangement studied here). However, it is important to note that the above equation is valid only when the tail index β of periods of inactivity is less than 1. In the experimental arrangement, the estimated tail index is $\beta = 1.14$ and the thin-tailed assumption of transport distances withstanding, equation (16), and not equation (17), will describe the dynamics of delta evolution. In systems which have tail index of the periods of inactivity less than 1, equation (17) describes the dynamics of evolution of the deltaic surface. Note that all the parameters of equation (17) are set by physical processes that govern the evolution of the deltaic surface: β is the tail index of the periods of inactivity, λ is set by the avulsion time scale of mean channel depths of the system, and D is a measure of the spread of the transport distances of sediment particles. In the case that the transport distances of sediment particles are heavy tailed with a tail index of $\kappa < 2$, the governing equation for surface elevation needs to be modified by replacing the $\partial^2/\partial x^2$ operator with a fractional $\partial^\kappa/\partial x^\kappa$ operator. The nature of the distribution of transport distances of sediment particles in a fan-delta system is a subject that needs further study.

[35] Let us denote by $S(t)$ the sediment surface elevation of the stratigraphic column, that is, the summation of all bed thicknesses recorded until clock time t has elapsed, given by [*Schumer and Jerolmack*, 2009]

$$S(t) = \sum_{i=0}^{N_t} d_{st}(i), \tag{18}$$

where $d_{st}(i)$ is the bed thickness recorded and N_t is the number of stratigraphic strata recorded in a given time interval [0, t]. *Schumer and Jerolmack* [2009] derive and describe the governing equation for the location of the sediment surface elevation, $S(t)$, of the stratigraphic column in the case when heavy-tailed hiatuses are present in the system. In section 5 we provided evidence for the existence of heavy-tailed hiatuses (τ_{st}) and the exponential distribution of the bed thickness (D_{st}). These two findings together lead us to the following governing equation for the location of sediment surface elevation:

$$\frac{\partial S}{\partial t} + e^{-\lambda' t}\frac{\partial^{\beta'}}{\partial t^{\beta'}}\left(e^{\lambda' t}S\right) - \lambda'^{\beta'}S = -V\frac{\partial S}{\partial z} + D'\frac{\partial^2 S}{\partial z^2}, \tag{19}$$

where S is the sediment surface elevation, β' is the tail index and λ' is rate of the exponential tempering of the hiatuses τ_{st}, V is the average rate of accumulation, D' is the diffusivity coefficient which describes the spread of accumulation rate around its mean and z is the vertical coordinate measured in the direction of the stratigraphic column. The tail index of τ_{st} which was found to be less than 1 and the exponential bed thickness distribution call for a tempered anomalous diffusion equation to describe the evolution of sediment surface elevation of the stratigraphic column. The governing equations in the case of constant accumulation rates and power law, heavy-tailed pdfs without truncation are discussed by *Schumer and Jerolmack* [2009].

9. Conclusions

[36] In this paper, we used high-resolution temporal data collected from a Delta Basin experiment conducted at the St. Anthony Falls Laboratory, University of Minnesota to fully characterize the statistics of surface elevation dynamics in depositional systems. The following conclusions were drawn from the present study.

[37] 1. We showed that the magnitudes of surface elevation increments, deposition (D_i) and erosion (E_i), are well approximated by truncated Pareto distributions where the upper bounds in both cases are governed by the maximum depths of the channels on the actively deforming surface of the system.

[38] 2. The magnitudes of depositional events (D_e) and erosional events (E_e), which were defined as the random sum of the magnitudes of elevation increments over their

respective durations of deposition (τ_d) and erosion (τ_e), were found to be well described by a truncated Pareto distribution with a thinner tail than that of D_i and E_i, indicating that the random variables which govern the stratigraphic column thickness need not always reflect the heavy-tailed nature of surface elevation dynamics.

[39] 3. The periods of inactivity (τ_i), which were shown to be the dominant time scale of the system, were found to be well approximated by a truncated Pareto distribution whose upper bound coincides with the avulsion time scale of the mean channel depth, thus allowing for a physical interpretation of the fitted parameters.

[40] 4. The hiatus lengths (τ_{st}) or the time intervals demarcating the stratigraphic deposits were shown to carry the signature of the heavy-tailed periods of inactivity and were found to be well approximated by a truncated Pareto distribution with a tail index of $\hat{\beta}' = 0.7$ and upper bound which corresponds to the avulsion time scale of the deepest channels in the system. The heavy-tailed hiatuses influence estimated rates of deposition and sediment surface evolution and provide support for the hypothesis of *Schumer and Jerolmack* [2009] that the bias in estimated deposition rates arise from heavy-tailed hiatus lengths.

[41] 5. It was shown that the bed thickness or the thickness of the preserved stratigraphy (D_{st}) is well approximated by an exponential distribution, indicating that the heavy-tailed nature of surface dynamics is apparently not preserved in the stratigraphic column.

[42] 6. It was shown that the governing equations for the surface elevation ($h(t)$) and sediment surface elevation ($S(t)$) of the stratigraphic column can be described by tempered anomalous diffusion equations [*Meerschaert et al.*, 2008] where the time-fractional derivative captures the heavy-tailed nature of the periods of inactivity and the hiatus lengths, respectively.

[43] 7. Finally, it was shown that all the truncation scales on the random variables studied are set either by the channel depths (space statistics) or the characteristic avulsion time scales of the channels (time statistics), indicating that channel depths act as a first-order control on the structure of surface dynamics and preserved stratigraphy in depositional systems.

Appendix A: Geometrical Interpretation of Multifractal Analysis

[44] The local singularity of a function at location t_0 is quantified using the so-called Hölder exponent defined as

$$|f(t_0) - f(t_0 + \epsilon)| \sim C|\epsilon|^{\mathcal{H}(t_0)}, \tag{A1}$$

where $0 < \mathcal{H}(t_0) < 1$ is the Hölder exponent of the function f at a location t_0 [*Muzy et al.*, 1994]. As seen in the above equation, the limit of $\mathcal{H} = 0$ corresponds to discontinuity in the signal and $\mathcal{H} = 1$ corresponds to discontinuity in the derivative of the signal. As $\mathcal{H} \to 0$ the signal is said to be more irregular or "rougher." The spectrum of Hölder exponents (also called the spectrum of singularities), $D(\mathcal{H})$, is defined as the Hausdorff dimension of all the points t in the signal which have the same Hölder exponent [*Parisi and Frisch*, 1985; *Bacry et al.*, 1993; *Jaffard*, 1997], that is,

$$D(\mathcal{H}) = d_{\mathcal{H}}\{t : \mathcal{H}(t) = \mathcal{H}\}. \tag{A2}$$

The scaling exponent function, $\zeta(q)$, and the spectrum of Hölder exponents, $D(\mathcal{H})$, are related through the Legendre transform given as [*Muzy et al.*, 1994; *Venugopal et al.*, 2006]

$$D(\mathcal{H}) = \min_q \{q\mathcal{H} - \zeta(q) + D_f\}, \tag{A3}$$

where D_f is the fractal dimension of the support of singularities of the function $f(t)$. For the case of a continuously differentiable $\zeta(q)$, the following relations hold

$$\mathcal{H} = \frac{d\zeta(q)}{dq} \tag{A4a}$$

$$D(\mathcal{H}) = q\mathcal{H} - \zeta(q) + 1, \tag{A4b}$$

thus providing a means of computing the spectrum of Hölder exponents from the scaling exponent function $\zeta(q)$. (Equation (A4b) is consistent with equation (A3) and, in fact, in view of equation (14), $D_f = 1 - c_0$.) Notice that when $\zeta(q)$ has a linear dependence on q (monofractality) the value of the Hölder exponent is a constant for all locations t (and $D(\mathcal{H})$ is a spike) indicating a homogeneous arrangement of local singularities in the signal. However, when $\zeta(q)$ has a nonlinear dependence on q (multifractality), more than one singularity is present in the signal which is characterized by a whole $D(\mathcal{H})$ spectrum of Hölder exponents, thus indicating a heterogeneous spread of various degrees of singularities across the signal. This heterogeneity of singularity arrangement manifests itself visually as spikes of varied strength heterogeneously arranged in the signal (as seen in Figure 3).

[45] In this study we used the higher-order structure function analysis to estimate the scaling exponent function and, by taking the Legendre transform, equation (A4), estimate the spectrum of Hölder exponents (as shown in Figure 14c). More sophisticated methods for the computation of the spectrum of Hölder exponents from the data are available via Wavelet Transform Modulus Maxima (WTMM) and Cumulant analysis (see *Venugopal et al.* [2006] for a detailed description of these methods). For example, the WTMM method (applied to the maxima of the wavelet coefficients only and not to the whole signal) allows computation of statistical moments of negative order and thus it has direct access to the right part of the spectrum of singularities. However, in our case the quadratic approximation of the spectrum of scaling exponents curve provides an excellent approximation to the empirically computed spectrum (see Figure 14b) allowing thus an accurate approximation of the right part of the spectrum of singularities due to its parabolic symmetric shape.

Notation

t time.
$h(t)$ elevation time series of experimental data.
$\delta h(t)$ elevation increments in time.

D_i positive elevation increments, $\delta h(t) > 0$.
E_i magnitude of negative elevation increments, $\delta h(t) < 0$.
τ_i periods of inactivity.
τ_e durations of erosional events.
τ_d durations of depositional events.
D_e magnitude of depositional events.
E_e magnitude of erosional events.
D_{st} thickness of stratigraphic deposits.
τ_{st} time interval demarcating the boundaries of the deposit D_{st}.
T_A time scale of avulsion.
σ_A net aggradation rate.
η depth of actively deforming channel.
$\hat{\alpha}_1$ tail index of fitted truncated Pareto distribution to D_i.
$\hat{\alpha}_2$ tail index of fitted truncated Pareto distribution to E_i.
$\hat{\alpha}'_1$ tail index of fitted truncated Pareto distribution to D_e.
$\hat{\alpha}'_2$ tail index of fitted truncated Pareto distribution to E_e.
$\hat{\beta}$ tail index of fitted truncated Pareto distribution to τ_i.
$\hat{\beta}'$ tail index of fitted truncated Pareto distribution to τ_{st}.
$\hat{\nu}$ upper bound of fitted truncated Pareto distribution to τ_i.
$\hat{\nu}'$ upper bound of fitted truncated Pareto distribution to τ_{st}.
$\hat{\gamma}$ lower bound of fitted truncated Pareto distribution to τ_i.
$M(q, r)$ qth order structure functions at a time scale of r.
H Hurst exponent.
$\zeta(q)$ scaling exponent function.
c_1 multifracral parameter and measure of the most prevailing Hurst exponent.
c_2 intermittency parameter.
c_0 multifractal parameter which quantifies the intercept of the $\zeta(q)$ curve.
D_0 fractal dimension of the elevation time series.
D_f fractal dimension of the support of singularities.
ϕ power law exponent of power spectral density.
D diffusivity of elevation increments.
λ rate of exponential tempering in periods of inactivity.
λ' rate of exponential tempering in hiatuses.
V average rate of accumulation of stratigraphic column.
D' diffusivity of rate of accumulation of stratigraphic column.
x distance along the flow paths.
z vertical axis coordinate measured along the stratigraphic column.
$\mathcal{H}$ Hölder exponent.
$D(\mathcal{H})$ Spectrum of Hölder exponent.

[46] **Acknowledgments.** This research was supported by the National Center for Earth-surface Dynamics (NCED), a Science and Technology Center funded by NSF under agreement EAR-0120914, and also by NSF grants EAR-0824084 and EAR-0835789. Stimulating discussions with Elizabeth Hajek, Mark Meerschaert, Rina Schumer, and Doug Jerolmack greatly helped in improving the ideas presented in this manuscript. Finally, we would like to thank B. A. Sheets and J. M. Kelberer for conducting the experiment discussed in this manuscript and for making their data publicly available.

References

Aban, I. B., M. M. Meerschaert, and A. K. Panorska (2006), Parameter estimation for the truncated Pareto distribution, *J. Am. Stat. Assoc.*, *101*(473), 270–277.

Ager, D. V. (1973), *The Nature of the Stratigraphic Record*, 114 pp., John Wiley, New York.

Alexander, J., and M. R. Leeder (1987), Active tectonic control on alluvial architecture, in *Recent Developments in Fluvial Sedimentology*, edited by F. G. Ethridge, R. M. Flores, and M. D. Harvey, *Spec. Publ. Soc. Econ. Paleontol. Mineral.*, *39*, 243–252.

Allen, J. R. L. (1978), Studies in fluviatile sedimentation: An exploratory quantitative model for the architecture of avulsion-controlled alluvial sites, *Sediment. Geol.*, *26*, 617–644.

Allen, P. A. (2008), Time scales of tectonic landscapes and their sediment routing systems, in *Landscape Evolution: Denudation, Climate and Tectonics Over Different Time and Space Scales*, edited by K. Gallager, S. J. Jones, and J. Wainwright, *Geol. Soc. Spec. Publ.*, *296*, 7–28.

Arneodo, A., E. Bacry, and J. F. Muzy (1998), Towards log-normal statistics in high Reynolds number turbulence, *Eur. Phys. J. B*, *1*, 129–140.

Bacry, E., J. F. Muzy, and A. Arneodo (1993), Singularity spectrum of fractal signals from wavelet analysis: Exact analysis, *J. Stat. Phys.*, *70*, 635–674.

Bradley, D., N. G. E. Tucker, and D. A. Benson (2010), Fractional dispersion in a sand bed river, *J. Geophys. Res.*, *115*, F00A09, doi:10.1029/2009JF001268.

Bruno, R., L. Sorriso-Valvo, V. Carbone, and B. Bavassano (2004), A possible truncated-Lévy-flight statistics recovered from interplanetary solar-wind velocity and magnetic-field fluctuations, *Europhys. Lett.*, *66*(1), 146–152.

Cartea, A., and D. del-Castillo-Negrete (2007), Fluid limit of the continuous time random walk with general Lévy jump distribution functions, *Phys. Rev. E*, *76*, 041105, doi:10.1103/PhysRevE.76.041105.

Clauset, A., C. R. Shalizi, and M. E. J. Newman (2009), Power law distributions in empirical data, *SIAM Rev.*, *51*(4), 661–703.

Foufoula-Georgiou, E., and C. P. Stark (2010), Introduction to special section on Stochastic Transport and Emergent Scaling on Earth's Surface: Rethinking geomorphic transport-Stochastic theories, broad scales of motion and nonlocality, *J. Geophys. Res.*, *115*, F00A01, doi:10.1029/2010JF001661.

Foufoula-Georgiou, E., V. Ganti, and W. E. Dietrich (2010), A nonlocal theory for sediment transport on hillslopes, *J. Geophys. Res.*, *115*, F00A16, doi:10.1029/2009JF001280, 2010.

Ganti, V., A. Singh, P. Passalacqua, and E. Foufoula-Georgiou (2009), Subordinated Brownian motion model for sediment transport, *Phys. Rev. E*, *80*, 011111, doi:10.1103/PhysRevE.80.011111.

Ganti, V., M. M. Meerschaert, E. Foufoula-Georgiou, E. Viparelli, and G. Parker (2010), Normal and anomalous diffusion of gravel tracer particles in rivers, *J. Geophys. Res.*, *115*, F00A12, doi:10.1029/2008JF001222.

Hajek, E. A., P. L. Heller, and B. A. Sheets (2010), Significance of channel-belt clustering in alluvial basins, *Geology*, *38*, 535–538.

Harman, C. J., D. M. Reeves, B. Baeumer, and M. Sivapalan (2010), A subordinated kinematic wave equation for heavy-tailed flow responses from heterogeneous hillslopes, *J. Geophys. Res.*, *115*, F00A08, doi:10.1029/2009JF001273.

Hooke, R. Le B. (1968), Model geology: prototype and laboratory streams: discussion, *Geol. Soc. Am. Bull.*, *79*, 391–394.

Jaffard, S. (1997), Multifractal formalism for functions: 1. Results valid for all functions, *SIAM J. Math. Anal.*, *28*, 944–970.

Kolmogorov, A. N. (1951), Solution of a problem in probability theory connected with the problem of the mechanism of stratification, *Trans. Am. Math. Soc.*, *53*, 171–177.

Leeder, M. R. (1978), A quantitative stratigraphic model for alluvium, with special reference to channel deposit density and interconnectedness, in *Fluvial Sedimentology*, edited by A. D. Miall, *Mem. Can. Soc. Pet. Geol.*, *5*, 587–596.

Mackey, S. D., and J. S. Bridge (1995), Three-dimensional model for alluvial stratigraphy: Theory and application, *J. Sediment. Res., Sect. B*, *65*, 7–31.

Meerschaert, M. M., and H.P. Scheffler (2004), Limit theorems for continuous time random walks with infinite mean waiting times. *J. Appl. Probab.*, *41*, 623–638.

Meerschaert, M. M., D. A. Benson, and B. Baeumer (1999), Multidimensional advection and fractional dispersion, *Phys. Rev. E*, *59*, 5026–5028, doi:10.1103/PhysRevE.59.5026.

Meerschaert, M. M., Y. Zhang, and B. Baeumer (2008), Tempered anomalous diffusion in heterogeneous systems, *Geophys. Res. Lett.*, *35*, L17403, doi:10.1029/2008GL034899.

Mohrig, D., P. L. Heller, C. Paola, and W. J. Lyons (2000), Interpreting avulsion process from ancient alluvial sequences: Gaudalope-Matarranya

system (northern Spain) and Wasatch Formation (western Colorado), *Geol. Soc. Am. Bull.*, *112*, 1787–1803.
Muzy, J. F., E. Bacry, and A. Arneodo (1994), The multifractal formalism revisited with wavelets, *Int. J. Bifurcat. Chaos*, *4*, 245–302.
Paola, C. (2000), Quantitative models of sedimentary basin filling, *Sedimentology*, *47*, 121–178.
Paola, C., and V. R. Voller (2005), A generalized Exner equation for sediment mass balance, *J. Geophys. Res.*, *110*, F04014, doi:10.1029/2004JF000274.
Paola, C., P. L. Heller, and C. L. Angevine (1992), The large-scale dynamics of grain-size variation in alluvial basins, 1: Theory, *Basin Res.*, *4*, 73–90.
Paola, C., K. Straub, D. Mohrig, and L. Reinhardt (2009), The "unreasonable effectiveness" of stratigraphic and geomorphic experiments, *Earth Sci. Rev.*, *97*, 1–43.
Parisi, G., and U. Frisch (1985), On the singularity structure of fully developed turbulence, in *Turbulence and Predictability in Geophysical Fluid Dynamics*, edited by M. Ghil, R. Benzi, and G. Parisi, pp. 84–88, Elsevier, New York.
Pelletier, J. D., and D. L. Turcotte (1997), Synthetic stratigraphy with a stochastic diffusion model of fluvial sedimentation, *J. Sediment. Res.*, *67*, 1060–1067.
Pyrcz, M. J., O. Catuneanu, and C. V. Deutsch (2005), Stochastic surface-based modeling of turbidite lobes, *AAPG Bull.*, *89*, 177–191.
Rosiński, J. (2007), Tempering stable processes, *Stochastic Processes Appl.*, *117*, 677–707.
Sadler, P. M. (1981), Sediment accumulation rates and the completeness of stratigraphic sections, *J. Geol.*, *89*, 569–584.
Schumer, R., and D. J. Jerolmack (2009), Real and apparent changes in sediment deposition rates through time, *J. Geophys. Res.*, *114*, F00A06, doi:10.1029/2009JF001266.
Schumer, R., D. A. Benson, M. M. Meerschaert, and B. Baeumer (2003), Fractal mobile/immobile solute transport, *Water Resour. Res.*, *39*(10), 1296, doi:10.1029/2003WR002141.
Schumer, R., M. M. Meerschaert, and B. Baeumer (2009), Fractional advection-dispersion equations for modeling transport at the Earth surface, *J. Geophys. Res.*, *114*, F00A07, doi:10.1029/2008JF001246.
Sheets, B., T. A. Hickson, and C. Paola (2002), Assembling the stratigraphic record: Depositional patterns and time-scales in an experimental alluvial basin, *Basin Res.*, *14*, 287–301.
Sheets, B., C. Paola, and J. M. Kelberer (2007), Creation and preservation of channel-form sand bodies in an experimental alluvial basin, *Sedimentary Processes, Environments and Basins*, edited by G. Nichols, E. Williams, and C. Paola, pp. 555–567, Blackwell, Oxford, U. K.
Stark, C. P., E. Foufoula-Georgiou, and V. Ganti (2009), A nonlocal theory of sediment buffering and bedrock channel evolution, *J. Geophys. Res.*, *114*, F01029, doi:10.1029/2008JF000981.
Straub, K. M., C. Paola, D. Mohrig, M. A. Wolinsky, and T. George (2009), Compensational stacking of channelized sedimentary deposits, *J. Sediment. Res.*, *79*, 673–688.
Straub, K. M., V. Ganti, C. Paola, and E. Foufoula-Georgiou (2010), Persistence of exponential bed thickness distributions in the stratigraphic record: Experiments and theory, Abstract EP44C-05 presented at 2010 Fall Meeting, AGU, San Francisco, Calif., 13–17 Dec.
Strong, N., and C. Paola (2008), Valleys that never were: Time surfaces versus stratigraphic surfaces, *J. Sediment. Res.*, *78*, 579–593.
Turcotte, D. L. (1992), *Fractals and Chaos in Geology and Geophysics*, Cambridge Univ. Press, New York.
Venugopal, V., S. G. Roux, E. Foufoula-Georgiou, and A. Arneodo (2006), Revisiting multifractality of high-resolution temporal rainfall using a wavelet-based formalism, *Water Resour. Res.*, *42*, W06D14, doi:10.1029/2005WR004489.
Voller, V. R., and C. Paola (2010), Can anomalous diffusion describe depositional fluvial profiles?, *J. Geophys. Res.*, *115*, F00A13, doi:10.1029/2009JF001278.
Zhang, Y., D. A. Benson, and B. Baeumer (2007), Predicting the tails of breakthrough curves in regional-scale alluvial systems, *Ground Water*, *45*(4), 473–484.

C. Paola, E. Foufoula-Georgiou, and V. Ganti, St. Anthony Falls Laboratory and National Center for Earth-surface Dynamics, University of Minnesota, 2 Third Ave. SE, Minneapolis, MN 55414, USA. (efi@umn.edu)

K. M. Straub, Department of Earth and Environmental Sciences, Tulane University, 6823 St. Charles Ave., New Orleans, LA 70118, USA.